



Influence of rotation speed and axial force on the friction stir welding of AISI 410S ferritic stainless steel

Gerbson de Queiroz Caetano^{a,*}, Cleiton Carvalho Silva^a, Marcelo Ferreira Motta^a,
Hélio Cordeiro Miranda^a, Jesualdo Pereira Farias^a, Luciano Andrei Bergmann^b,
Jorge F. dos Santos^b

^a Universidade Federal do Ceará, “Department of Materials and Metallurgical Engineering”, Campus do Pici, Building 1080, 60440-554, Fortaleza, Ceará, Brazil

^b Helmholtz-Zentrum Geesthacht, Institute of Material Research, Material Mechanics, Solid State Joining Processes, Max Planck Strasse 1, 21502 Geesthacht, Schleswig-Holstein, Germany

ARTICLE INFO

Associate Editor: C.H. Caceres

Keywords:

Friction stir welding
Ferritic stainless steels
Axial force
Rotation speed
Defects

ABSTRACT

The Friction Stir Welding process parameters were varied to provide a combination of an acceptable surface finish, absence of cracks, and full tool penetration. Two levels of rotation speed and axial forces from 10 to 30 kN were applied, whilst keeping the welding speed constant at 1 mm/s. One of the defects analyzed was the production of flashes. This can occur due to an increase in axial force and because of the instability in its applications, which implies directly on the formation of volumetric defects along the stir zone. FSW joints without root flaws can be achieved through a correct balance between the axial force and rotation speed, which also allows a greater immersion of the tool probe in the joint. Both rotation speeds using an axial force of around 20 kN proved to be good welding parameters for the FSW process. The welding of the AISI 410S steel (under these conditions) resulted in joints without internal defects and with a good surface finish.

1. Introduction

Among the stainless steels, the ferritic family is characterized as having a substantially ferritic microstructure at room temperature and therefore has a body centered cubic (BCC) crystalline structure. The chromium content of these steels may range from 11 to 30% and it may also contain additions of Mo, Nb, Ti, among others. Smith (1993) noted that ferritic stainless steels provide approximately the same corrosion resistance but have lower ductility, toughness, and weldability when compared to austenitic stainless steels, which are the most frequently used commercially because of their good corrosion and mechanical strength properties. In addition, Kotecki and Lippold (2005) showed that ferritic stainless steels can be used in a wide variety of applications where resistance against pitting corrosion and/or stress corrosion cracking is more important than mechanical strength. Another great advantage of ferritic stainless steels is the reduction or absence of nickel in their composition, since nickel is one of the most expensive alloying elements and thus, increases considerably the price of austenitic stainless steels compared to ferritic stainless steels as reported by Silva et al. (2007).

The lack of applications for ferritic stainless steels is related to the

metallurgical problems resulting from the fusion welding of these steels. When submitted to its thermal cycles, these materials undergo metallurgical changes, which compromise their weldability and the mechanical or corrosion response of the welds. Toughness is especially affected as it is directly related to grain growth in the heat affected zone and fusion zone for autogenous welds. In addition, some secondary phases may be formed in the weld, affecting the corrosion resistance. Silva et al. (2006) evaluated the changes in the HAZ of a AISI 410S ferritic stainless steel submitted to different energy levels in a fusion welding process, and observed that in addition to the formation of martensite there were zones with grain growth, which causes a decrease in the toughness and compromises the mechanical resistance. Another problem verified was the precipitation of chromium nitrides and carbides finely dispersed in the HAZ, which cause embrittlement and intergranular corrosion.

In recent decades, friction stir welding (FSW), a solid-state welding process developed by The Welding Institute (TWI) of Cambridge in England, has revolutionized the joining of materials that were considered non weldable or difficult to weld. Mishra and Ma. (2005) reported that this process uses a non-consumable tool that rotates and translates the workpiece, resulting in heating and plastic deformation of

* Corresponding author.

E-mail address: gerbsonqueiroz@alu.ufc.br (G.d.Q. Caetano).

the materials to be joined. In this case, the material is heated to temperatures below those experienced in fusion welding.

Highlighted among the advantages commonly attributed to the FSW process are: the good strength and ductility of the welds, minimal residual stress and distortion, absence of defects related to melting of the material, smaller heat affected zone, and a grain refined microstructure that increases the tensile strength and fatigue life as propounded by Bilgin and Meran, (2012); Cavaliere et al. (2006) and Sathiya et al. (2006). In this process, the rotational speed and the axial force are the two parameters that are directly related to the generation of heat. A combination of welding speed, axial force and rotational speed are the key factors to obtain a balanced set of welding parameters. The correct adjustment of these parameters allows the joining of metals, especially those that present difficult weldability when traditional fusion processes are applied as observed by Silva et al. (2008). In the case of ferritic stainless steels, a low heat input and high welding speed are recommended to avoid ferritic grain growth and to form a refined microstructure. However, Bilgin and Meran. (2012) have shown that such characteristics can be achieved very well by using the FSW process. Therefore, this work aims to evaluate the effect of different FSW welding parameters on welding a AISI 410S ferritic stainless steel.

2. Materials and methods

The welds were carried out with 4-mm-thick plates of AISI 410S ferritic stainless steel. The chemical composition of the material was determined by optical emission spectroscopy and is presented in Table 1.

The samples were joined by the FSW process at the Helmholtz-Zentrum Geesthacht (HZG) in Germany. All welds were made using the HZG Gantry System with a butt joint configuration, as shown in Fig. 1. An inert gas injection system (Ar) was used to protect the material during the process, since at temperatures above 535 °C this stainless steel reacts with the atmosphere. The welds were carried out in the load control mode with an integrated system to record the process data, such as plunge depth, rotational speed, torque, forces applied to the tool and tool position over time.

A polycrystalline cubic boron nitride (PCBN) tool was used. The tool had a conical diameter of 25 mm and a conical pin with a diameter of 9.2 mm and a length of 3.7 mm. The pin had a conical surface with the presence of negative recesses, which were in the form of a spiral with respect to the axis of the symmetry of the tool.

In a previous work Muthukumaran and Mukherjee (2006) observed that the metal flow in FSW is caused by either the extrusion of metal around the tool probe or the frictional heat generated between the tool shoulder and the sample. Sinha et al. (2008) showed that as the intensity of the frictional contact between the tool shoulder and the work piece is one of the main factors responsible to eliminate defects, parameters such as axial force and rotation speed directly affect this metallic flow. In this work, six welding conditions were tested to evaluate the influence of the process parameters on the generation of heat and defect formation. Thus, the rotational speed was varied between 450 rpm and 800 rpm, with axial forces changing from 10 to 30 kN. For both rotational speeds used, the tool tilt angle was maintained at 0° and the welding speed was 1 mm/s as shown in Table 2.

These parameters were related to the energy of the process and the heat input generated during the FSW process. There are different ways

to calculate the heat generated during the FSW process. Eq. 1 shows the total equivalent energy required for joint consolidation. The frictional coefficient of the material, the pressure exerted by the tool, the rotation speed and the geometry of the tool used in the welding are sufficient components to determine this energy and it is calculated according to Deqing et al. (2004):

$$E_t = \pi \cdot \mu \cdot P_s \cdot V_r \cdot \frac{D^2 + D \cdot d + d^2}{45 \cdot (D + d)} \quad (1)$$

where E_t is the total equivalent heat input (kJ), μ is the friction coefficient of the material, P_s is the pressure exerted by the support on the material (Pa), V_r is the rotation speed (rad/s), D is the diameter of the shoulder, and d is the diameter of the pin (m). Another way to calculate the heat input in FSW is using Eq. 2 to determine the energy per unit length (Lienert et al., 2002):

$$E_l = \eta \cdot \frac{T \cdot V_r}{V_s} \quad (2)$$

Where E_l is the heat input per unit length (kJ/mm), η is the efficiency of the FSW process for steels, T the Torque (N.m), V_r the rotation speed (rad/s) and V_s the welding speed (mm/s).

3. Results and discussion

3.1. Rotation speed

The process parameters interfere directly in the heat input, which strongly influences the heating and cooling rates of the thermal cycle and consequently the resultant microstructure. However, the energy calculated based on the process parameters corresponds to an equivalent energy and not exactly to the energy produced during the process, since there are losses that were not considered, the main ones being conduction and convection in the region of the weld.

The rotation speed is the parameter related to the frictional force and friction at the interface between the material and the tool and is therefore directly linked to the heat generation during the welding process, as reported by Bilgin and Meran (2012) and Lakshminarayanan and Balasubramanian (2013). The frictional coupling of the tool surface with the joint governs the heating mechanism and the rotation of the tool results in agitation and mixing of the material around the probe. Thus, the higher the rotational speed, the higher the temperature in the process will be; this is due to the increase of the friction heating as propounded by Colegrove et al. (2007); Mishra and Ma (2005) and Uday et al. (2010).

The strong influence of the rotation speed on the heat generation can be seen among the welds of AISI 410S ferritic stainless steel produced by FSW in this work. The reduction in rotation speed from 800 to 450 rpm between Conditions 3 and 4, in which welding was performed with an axial force of around 20 kN, generated a drop in total heat input and heat input per unit length of around 0.4 kJ/mm, as shown in Fig. 2.

3.2. Axial force

Kim et al. (2006) analyzed the axial force and showed that instability in its application results in a lack of forging required to guarantee the consolidation of the joint and consequently leads to the formation of volumetric defects. The instabilities observed for Conditions 5 and 6 directly reflect the poor quality of these welds, a fact not

Table 1
Chemical composition of the material (% weight).

Material	Elements												
	C	Si	Mn	P	S	Cr	Ni	Mo	Cu	Co	N	Fe	
410S	0.025	0.37	0.30	0.023	< 0.010	12.8	0.21	0.01	0.21	0.02	0.033	Bal.	

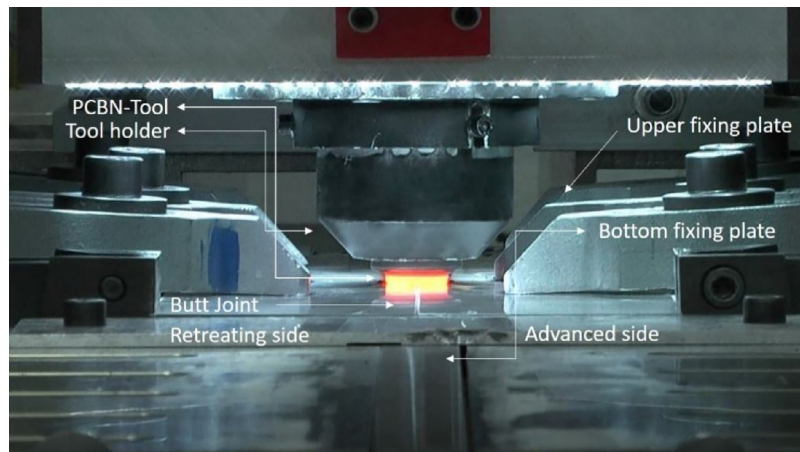


Fig. 1. Configuration of AISI 410S steel joints.

Table 2
Welding Parameters AISI 410S.

Condition	Rotation Speed (rpm)	Axial Force (kN)
1	800	30
2	800	25
3	800	22
4	450	20
5	450	15
6	450	10

observed for Condition 4 (Fig. 3). Therefore it is possible to infer that the increase of the force also produces a higher amount of heat in the process, which increases the temperature and the degree of softening of the material; however, although this force has less influence than the rotation speed, the heat input decreases as the force decreases.

The six curves of axial force initially exhibited a similar behavior. During the initial phase of the process, a pressure gradient emerged along the penetration channel, this variation occurs due to the different levels of contact between the tool and the surface of the joint and consequently of the area variation where the force is being applied. The increase of the pressure is counter balanced by the increase of the axial

force. After the tool reaches the desired depth of penetration, the pressure gradient decreases until it reaches a steady state. After reaching equilibrium, new abrupt changes in the curve of the axial force \times time characterize a nonuniformity of force application, compromising the flow of the material and resulting in the formation of defects.

An analysis of the welding parameters of the FSW process shows that the torque exerted by the tool increases with the increase of the axial force.

The torque for the AISI 410S ferritic stainless steel FSW joints for Condition 1 with an axial force of 30 kN, was higher than the torque for Condition 3 with a force of 22 kN. Therefore the greater the force, the greater the pressure of the tool on the material is, because a greater torque is necessary for the rotation of the tool, as shown in Fig. 4. In a previous work, Buchibabu et al. (2017) observed the same behavior. The rotation speed also causes changes in the torque due to the greater or lesser degree of plasticity of the metal caused by the changes of heat input, and therefore both the rotation speed and the applied axial force are determinant factors in the evolution of the torque during the FSW process, which is in agreement with the conclusions reported by Leita et al. (2012).

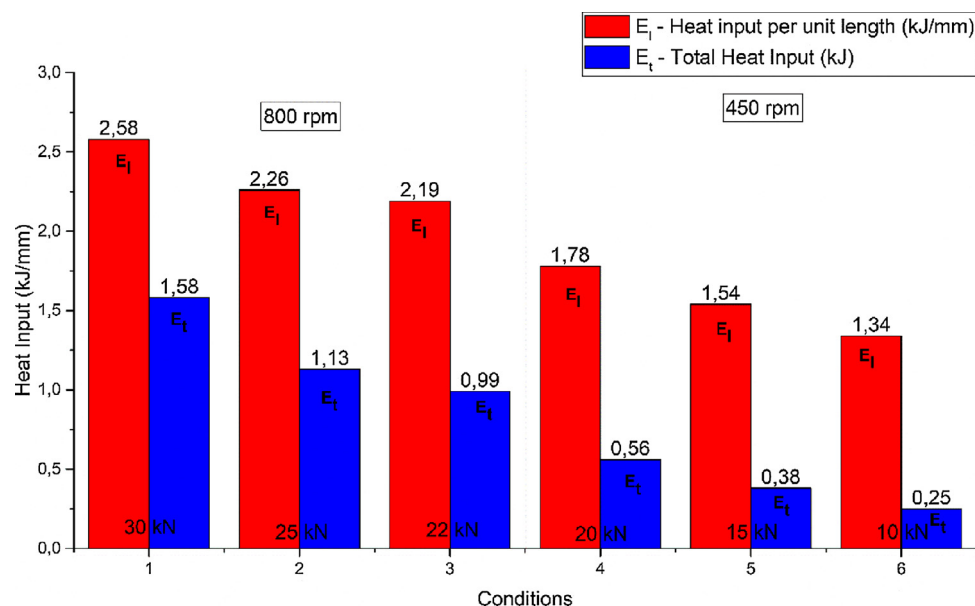


Fig. 2. Equivalent heat input per unit length (Eq. 2) and total heat input (Eq. 1) calculated for the different welding conditions applied to AISI 410S steel by the FSW process.

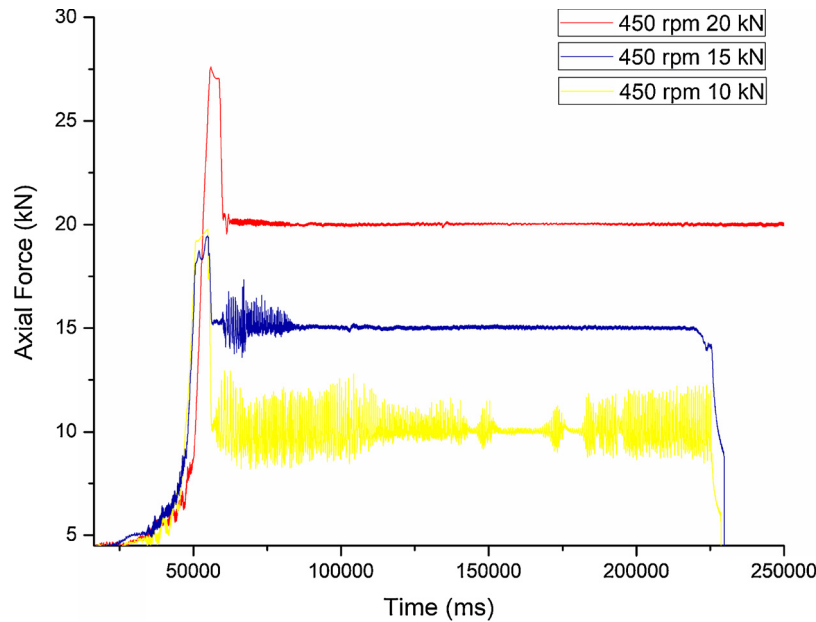


Fig. 3. Variation of the axial force during welding by the FSW process for AISI 410S steel.

3.3. Surface finish

An analysis of the surface of the AISI 410S steel welded joints obtained by FSW in this work shows that flashes are directly related to the increase of the axial force, which with a rotation speed of 800 rpm causes an increase in the heat input. As noted by Trueba et al. (2015), higher welding temperatures in FSW cause a decrease in viscosity and the displacement of a greater amount of material by the tool probe, which makes it more difficult for the shoulder to restrain the displaced metal and causes flash formation. The Fig. 5 shows in detail that the amount of flash decreases as the axial force decreases from 30 to 22 kN, and these flashes are more critical in the samples joined under Condition 1, which involved a higher axial force.

In the conditions where the weld was carried out with a rotational speed of 450 rpm, the presence of flashes was controlled in the conditions with the smallest forces, which can be seen in Conditions 5 and 6 where the axial forces of 15 and 10 kN, respectively, were applied

(Fig. 5). This occurred due to the instability of the axial force of the process, which caused irregularities in the stir zone and consequent material losses. According to the analysis of defects in FSW welds performed by Threadgill (2007), the production of flash can occur due to both high heat input and irregularities in the application of the axial force, generating an inadequate material flow with the formation of voids and loss of plasticized material.

No superficial cavities were observed in this work under the conditions evaluated despite the presence of surface depressions, due of the intense pressure exerted by the shoulder of the tool on the welded material, in Conditions 1 and 2, which were welded with the rotational speed of 800 rpm and the higher axial forces. These defects are associated to a lack of heat or excess of heat in the material during the welding process, which indicates that even under the conditions with the lowest rotation speed and, consequently, lower heat input, the heat generated in the region near the tool shoulder was sufficient to confer on the material a good viscosity and plasticity, which was not observed

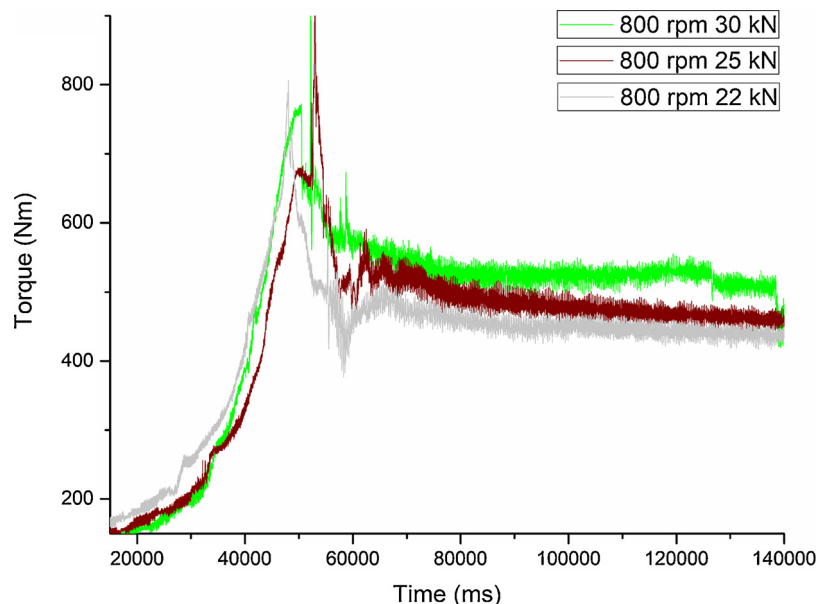


Fig. 4. Variation of the torque throughout the FSW process for AISI 410S steel.

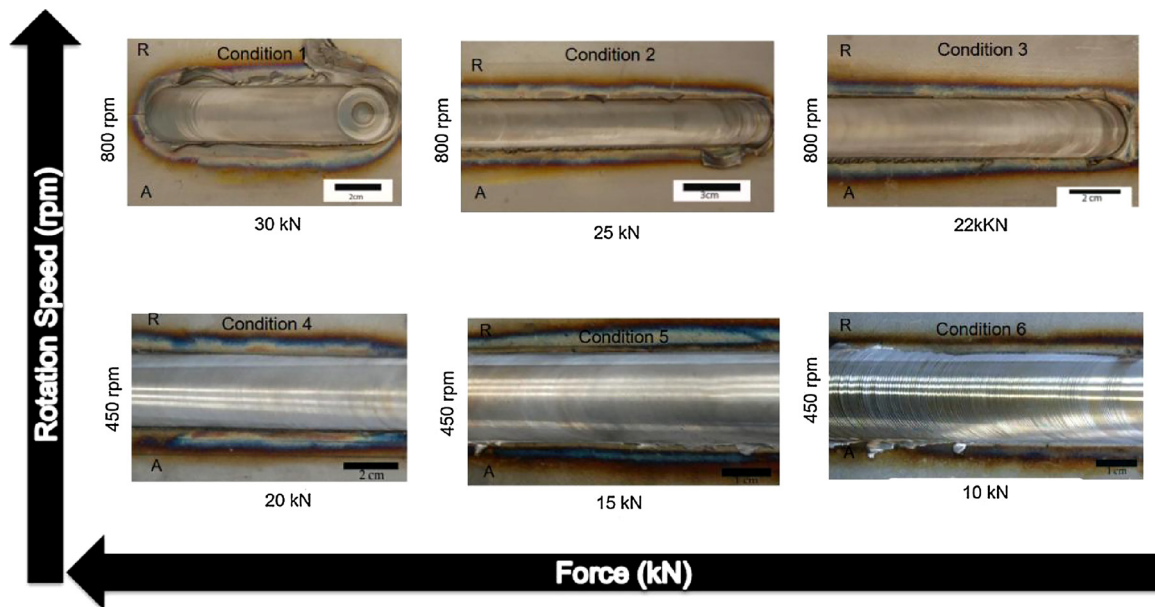


Fig. 5. Surface finishing of different FSW welds produced for AISI 410S steel as a function of the rotation speed and axial force applied.

in most internal regions close to the tool probe.

3.4. Defect analysis

The cross-section analysis of the FSW joints of the AISI 410S ferritic stainless steel verified the consolidation of FSW joints without defects for the two rotational speeds, 800 and 450 rpm. The material flow reached an adequate state of plasticization due to the heat intensity obtained by the combination of the parameters used; Kim et al. (2017) also observed similar results with FSW of a 430M2 ferritic stainless steel using a rotational speed of 900 rpm.

The macroscopic analysis of the cross-section of the FSW samples for Conditions 5 and 6 showed voids, in the samples welded with a rotation speed of 450 rpm and axial forces of 15 kN and 10 kN, respectively. This behavior as observed by Tongne et al. (2015) was attributed to a lower interaction between the tool and the material, due to the low axial force and as consequence reduced friction force and insufficient heat to achieve an adequate plasticizing state for material flow during the FSW process (Fig. 6). According to Doude et al. (2015), these voids in the stir zone in regions close to the root of the weld, as observed in Condition 5, indicate the use of parameters with values below the ideal set of welding parameters recommended for consolidation of a defect-free FSW joint, that is due to the use of a low rotation speed and low axial force.

An evaluation of the cross-sectional macrographs of the FSW welds reaffirmed the high flash formation and surface depression formed under Condition 1, when a rotation speed of 800 rpm and axial force of 30 kN were applied, as previously shown in the analysis of the surface finish presented in Fig. 5. As the axial force decreases to 25 and 22 kN, there is a decrease in the surface depression and flashes, as can be observed in Fig. 7.

Condition 1 shows the root flaws due to the high force that was applied. However, in conditions with a reduced axial force and rotation speed, these root flaws also occur, but they present different morphologies as shown in Fig. 8. The different morphologies of the root flaws formed occur due to the distinct mechanisms of defect formation, which can be formed either by virtue of an excess of axial force applied by forming a root flaw in the recess form due to the passage of the tool pin in a region below and between the joint and the backing bar as shown in Fig. 8(a). Nonetheless, root flaws can also be formed due to a decrease in the axial force and the rotation speed, which is attributed to

a lower interaction between the tool and the material, due to the low axial force and consequently a reduction of the friction force and necessary heat generation to achieve an adequate plasticizing state of the material flow. This inadequate plasticizing hinders the movement of the material around the tool and then difficult the consolidation of the stir zone during the FSW process. Thus, this particular kind of defect is characterized by the observation of a line, referring to the interface between the two plates of butt joint as shown in Fig. 8(b) and is associated with an insufficient penetration of the tool as reported by Edwards and Ramulu (2015).

The formation of root flaws with excess penetration or lack of penetration demonstrates that the production of AISI 410S ferritic stainless steel joints by the FSW process without root flaws should be carried out with not only an increase or decrease of the axial force, but also with an appropriated balance between axial force and angle of the tool, as reported by Shultz et al. (2010). An appropriated balance enables a greater immersion of the tool probe into the joint.

Although a correct balance between the tool angle and axial force is a way to consolidate FSW joints without root flaw defects, this can also be obtained with the correct balance between the axial force and rotation speed without the need to vary the angle of the tool, as has been shown in this study. Therefore, the relation between both rotational speeds and the axial force of 20 kN is important, as it was possible to obtain joints without defects with a tool angle of 0°; however it is not possible to state whether this combination is valid for different tool angles.

Under the conditions in which a rotation speed of 450 rpm was applied, the macroscopic analysis confirmed interferences in the application of axial force, revealing the presence of voids throughout the stir region, which was the most critical for Condition 6, in which an axial force of 10 kN was used (Fig. 9). This lack of filling or tunnel defect consists of internal regions of the welded joint without material, forming voids along the length of the weld. According to Mishra and Ma (2005), this is caused due to a lack of heat produced by the cold parameters, such as low rotational speeds and low axial forces, which generate less friction or less time of permanence of the tool on the material. Kumar and Kailas (2008) claim that in addition to low heating, the lack of shoulder pressure on the material also affects the flow, preventing it from filling the entire weld region.

Therefore, FSW joints of AISI 410S ferritic stainless steel with satisfactory surface finish and no defects in the stir zone can be obtained

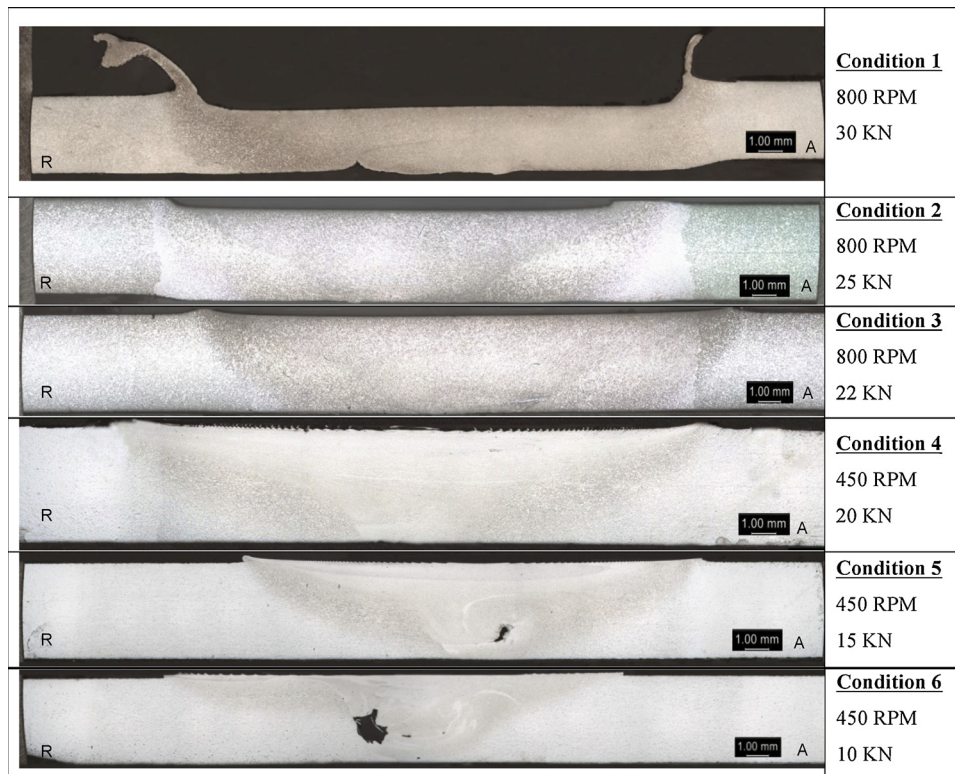


Fig. 6. Cross-sectional macrographs of different welded conditions of AISI 410S steel.

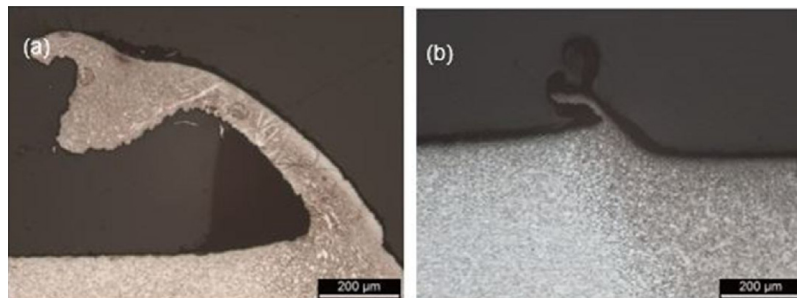


Fig. 7. (a) Flash Excess in Condition 1. (b) Flash Decrease in Condition 3. (50x).

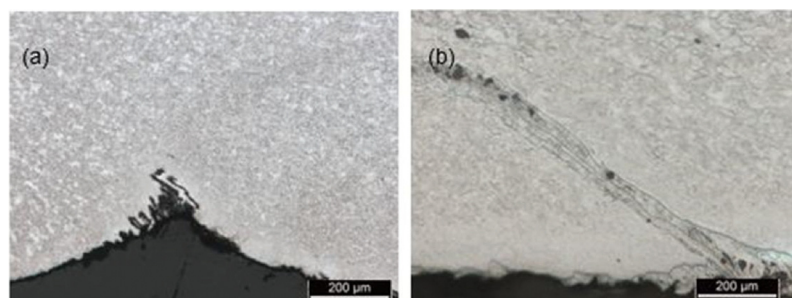


Fig. 8. (a) Root Flaws due to the excess penetration in Condition 1. (b) Root Flaws due to lack of penetration in Condition 2 (50x).

using parameters that ensure adequate heat intensity to plasticize the material flow, which can be obtained by increasing the rotational speed to 800 rpm; however, increasing the axial force to values higher than 25 kN is not advisable, because as well as accentuating the production of flashes it can lead to the formation of flaws in the root of the joint due to excess penetration.

4. Conclusions

Based on the experimental results of the parameters of the FSW process and their implications in the formation of defects for the welding of the AISI 410S ferritic stainless steel, it was possible to conclude that:

1 With the appropriate combination of welding parameters it was

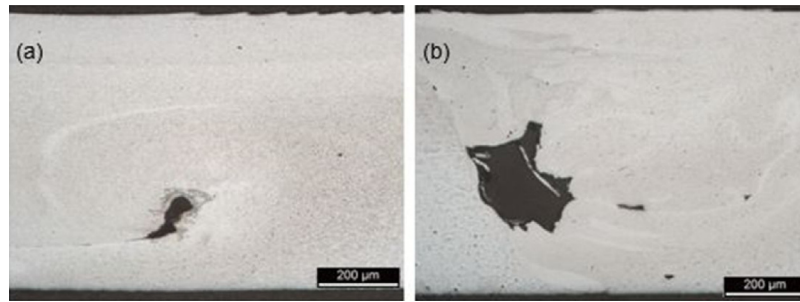


Fig. 9. (a) Worm hole in condition 5. (b) Voids and Worm hole in condition 6. (50x).

possible to weld the AISI 410S ferritic stainless steel successfully, producing a stable joint without defects.

- 2 Instability in the process leads to vibration and consequently a lack of forging of the material (that is visible in the force graph) during the movement of the tool to ensure consolidation of the joint and consequently results in the formation of volumetric defects along the stir zone.
- 3 The torque exerted by the tool decreases with the decrease in the force applied, because the smaller friction applied by rotation and force, the lower the tool pressure on the material and the less torque is required to consolidate the tool rotation.
- 4 The production of flash can occur with a increase in axial force, as this increases the heat input and allows the formation of a larger amount of plasticized material, and because of the instability of the application of axial force.
- 5 The production of joints in AISI 410S ferritic stainless steel welded by the FSW process without root flaws is achieved through a correct balance between the axial force and rotation speed, which also allows a greater immersion of the tool probe into the joint.
- 6 The best combinations of FSW parameters for the production of welded joints without defects were the combination of a rotation speed of 450 rpm with an axial force of 20 kN and a rotation speed of 800 rpm with an axial force of 22 kN. In both cases, the welding speed was maintained at 1 mm/s and with a tool angle of 0.

Acknowledgments

The authors would like to thank the Laboratório de Pesquisa e Tecnologia em Soldagem (LPTS) and the Helmholtz-Zentrum Geesthacht (HZG) as well as CNPq and FUNCAP for funding the project and the Department of Metallurgical and Materials Engineering of the Federal University of Ceará for the master's degree.

References

- Bilgin, M.B., Meran, C., 2012. The effect of tool rotational and traverse speed on friction stir weldability of AISI 430 ferritic stainless steels. *Mater. Des.* 33, 376–383.
- Buchibabu, V., Reddy, G.M., De, A., 2017. Probing torque, traverse force and tool durability in friction stir welding of aluminum alloys. *J. Mater. Process. Technol.* 241, 86–92.
- Cavaliere, P., Campanile, G., Panella, F., Squillace, A., 2006. Effect of welding parameters on mechanical and microstructural properties of AA6056 joints produced by friction stir welding. *J. Mater. Process. Technol.* 180, 263–270.
- Colegrove, P.A., Shercliff, H.R., Zettler, R., 2007. Model for predicting heat generation and temperature in friction stir welding from the material properties. *Sci. Technol. Weld. Join.* 12, 284–297.
- Deqing, W., Shuhua, L., Zhaoxia, C., 2004. Study of friction stir welding of aluminum. *J. Mater. Sci.* 39, 1689–1693.
- Doude, H., Schneider, J., Patton, B., Stafford, S., Waters, T., Varner, C., 2015. Optimizing weld quality of a friction stir welded aluminum alloy. *J. Mater. Process. Technol.* 222, 188–196.
- Edwards, P.D., Ramulu, M., 2015. Material flow during friction stir welding of Ti-6Al-4V. *J. Mater. Process. Technol.* 218, 107–115.
- Kim, Y.G., Fujii, H., Tsumura, T., Komazaki, T., Nakata, K., 2006. Three defect types in friction stir welding of aluminum die casting alloy. *Mater. Sci. Eng. A* 415, 250–254.
- Kim, K.H., Bang, H.S., Kaplan, A.F.H., 2017. Joint properties of ultra thin 430M2 ferritic stainless steel sheets by friction stir welding using pinless tool. *J. Mater. Process. Technol.* 243 (May), 381–386.
- Kotecki, D.J., Lippold, J.C., 2005. *Welding Metallurgy and Weldability of Stainless Steels*. John Wiley & Sons, New Jersey, USA.
- Kumar, K., Kailas, S.V., 2008. The role of friction stir welding tool on material flow and weld formation. *Mater. Sci. Eng. A* 485, 367–374.
- Lakshminarayanan, A.K., Balasubramanian, V., 2013. Process parameters optimisation for friction stir welding of AISI 409M grade ferritic stainless steel. *Exp. Tech.* 37, 59–73.
- Leitao, C., Louro, R., Rodrigues, D.M., 2012. Using torque sensitivity analysis in accessing friction stir Welding/Processing conditions. *J. Mater. Process. Technol.* 212, 2051–2057.
- Liener, T.J., Stellwag Jr, W., Lehman, L., 2002. Comparison of heat inputs: friction stir welding vs. Arc welding. *Am. Weld. Soc.* 1–3.
- Mishra, R.S., Ma, Z.Y., 2005. Friction stir welding and processing. *Mater. Sci. Eng. R Rep.* 50, 1–78.
- Muthukumar, S., Mukherjee, S.K., 2006. Two modes of metal flow phenomenon in friction stir welding process. *Sci. Technol. Weld. Join.* 11, 337–340.
- Sathya, P., Aravindan, S., Haq, A.N., 2006. Effect of friction welding parameters on mechanical and metallurgical properties of ferritic stainless steel. *Int. J. Adv. Manuf. Technol.* 31, 1076–1082.
- Shultz, E.F., Cole, E.G., Smith, C.B., Zinn, M.R., Ferrier, N.J., Pfefferkorn, F.E., 2010. Effect of compliance and travel angle on friction stir welding with gaps. *J. Manuf. Sci. Eng.* 132, 41010.
- Silva, C.C., Neto, J.A., Sant'ana, H., Farias, J.P., 2006. Alterações microestruturais na ZAC do aço inoxidável ferrítico 410S-efeitos sobre a resistência à corrosão. *Soldad. Insp.* 11.
- Silva, C.C., Machado, J.P.S.E., Sobral-Santiago, A.V.C., de Sant'Ana, H.B., Farias, J.P., 2007. High-temperature hydrogen sulfide corrosion on the heat-affected zone of the AISI 444 stainless steel caused by Venezuelan heavy petroleum. *J. Pet. Sci. Eng.* 59, 219–225.
- Silva, C.C., Farias, J.P., Miranda, H.C., Guimarães, R.F., Menezes, J.W.A., Neto, M.A.M., 2008. Microstructural characterization of the HAZ in AISI 444 ferritic stainless steel welds. *Mater. Charact.* 59, 528–533.
- Sinha, P., Muthukumar, S., Mukherjee, S.K., 2008. Analysis of first mode of metal transfer in friction stir welded plates by image processing technique. *J. Mater. Process. Technol.* 197, 17–21.
- Smith, W.F., 1993. *Structure and Properties of Engineering Alloys*, 2nd edition. McGraw-Hill, New York.
- Threadgill, P.L., 2007. Terminology in friction stir welding. *Sci. Technol. Weld. Join.* 12, 357–360.
- Tongne, A., Jahazi, M., Feulvarch, E., Desrayaud, C., 2015. Banded structures in friction stir welded Al alloys. *J. Mater. Process. Technol.* 221, 269–278.
- Trueba, L., Heredia, G., Rybicki, D., Johannes, L.B., 2015. Effect of tool shoulder features on defects and tensile properties of friction stir welded aluminum 6061-T6. *J. Mater. Process. Technol.* 219, 271–277.
- Uday, M.B., Ahmad Fauzi, M.N., Zuhailawati, H., Ismail, A.B., 2010. Advances in friction welding process: a review. *Sci. Technol. Weld. Join.* 15, 534–558.